Journal of Thermal Analysis and Calorimetry
https://doi.org/10.1007/s10973-024-13318-x

Kinetic analysis of reversible solid-gas reactions in films: application to the decomposition of $CaCO_3$ and $BaCO_3$ carbonates

Daniel Sanchez-Rodriguez[1] · Sihem Zaidi[1,2] · Genis Riera[1] · Anna Planella[1] · Mohamed Dammak[2] · Pere Roura-Grabulosa[1] · Jordi Farjas[1]

Received: 11 October 2023 / Accepted: 19 May 2024

Abstract
To determine the decomposition conditions of carbonates in the form of films, we investigated the dependence of the kinetics on carbon dioxide partial pressure, temperature and film thickness. Three different analyses allow us to determine the functional dependence of the decomposition onset temperature on the CO_2 partial pressure, of the reaction rate on the temperature and of the kinetics on the film thickness. The latter analysis also reveals geometrical aspects of the reaction mechanism. Experiments have been carried out with $CaCO_3$ and $BaCO_3$ films. The simple geometry of the films and their relatively fast heat and gas transport allow the reaction kinetics to be easily explored.

Keywords Reversible reactions · Carbonate decomposition · Films · Thermogravimetry

Introduction

A large number of studies are devoted to the thermal decomposition of alkaline earth metal carbonates due to their multiple applications [1–3]. For example, the decomposition of $CaCO_3$ is widely studied for the production of quicklime and concrete [4, 5], CO_2 capture [6–8] and energy storage [9–11]. In addition, $BaCO_3$ is also used in the synthesis of concrete [12]. Moreover, the thermal decomposition of $BaCO_3$ is a crucial step in the synthesis of high-temperature superconductors [13], ferroelectric and dielectric materials [14, 15]. Therefore, knowing the decomposition temperature of a carbonate, as well as its functional dependence on the system parameters, is of interest for many practical situations.

The decomposition of carbonates is a reversible reaction,

$$MCO_3(s) \rightleftharpoons MO(s) + CO_2(g), \quad (1)$$

so its kinetics depends on the partial pressure of CO_2 [1]. The partial pressure of CO_2 at the interface depends on the transport of CO_2 through the sample and on the surrounding atmosphere. For instance, at atmospheric pressure, the formation of a stagnant CO_2 layer around particles can slow down the decomposition [2, 16, 17]. As a result, the decomposition kinetics depends on the morphology of the material [18–20], the gas flow rate [21], the total pressure and the composition of the atmosphere [1]. Consequently, a wide dispersion of activation energy values has been reported; from 155 to 960 kJ mol^{-1} for $CaCO_3$ [2, 3, 22] and from 226 to 305 kJ mol^{-1} for $BaCO_3$ [23–28].

Thermal decomposition of metal carbonates is a thermally activated process and for low or moderate values of $p(CO_2)$ can be approximately described by a single step kinetics [1, 29, 30]:

$$\frac{d\alpha}{dt} = A e^{-\frac{E_A}{R_G T}} f(\alpha) g(p(CO_2)), \quad (2)$$

where t is the time, T is the temperature, α is the degree of transformation ($0 \le \alpha \le 1$), E_A and A are the activation energy and the pre-exponential term of the rate constant, respectively, R_G is the universal gas constant, $p(CO_2)$ is the partial pressure of CO_2, $f(\alpha)$ is a characteristic function of the reaction model [21] and $g(p(CO_2))$ is a function that accounts for the dependence on $p(CO_2)$ [1, 2]. For reversible

✉ Jordi Farjas
jordi.farjas@udg.edu

[1] Physics, Universitat de Girona, Campus Montlivi, Edif. PII, 17003 Girona, Catalonia, Spain

[2] Laboratoire de Chimie Inorganique, Faculté des Sciences de Sfax, University of Sfax, BP 1171, 3000 Sfax, State, Tunisia

Published online: 17 July 2024

reactions such as the decomposition of a carbonate, the most common dependence on $p(CO_2)$ is [2, 21, 28]:

$$g(p(CO_2)) = 1 - \frac{p(CO_2)}{p_{eq}(CO_2)}, \quad (3)$$

where $p_{eq}(CO_2)$ is the equilibrium partial pressure in atm. $p_{eq}(CO_2)$ depends on temperature through the standard Gibbs free energy change, ΔG^0:

$$\ln(p_{eq}(CO_2)) = -\frac{\Delta G^0}{R_G T}. \quad (4)$$

In the case of $CaCO_3$ and $BaCO_3$ decompositions, ΔG^0 exhibits a linear temperature dependence for a wide temperature range,

$$\Delta G^0 = a - bT, \quad (5)$$

where $a = 171\ kJ\ mol^{-1}$ and $b = 0.147\ kJ\ K^{-1}\ mol^{-1}$ for the decomposition of $CaCO_3$ [29, 31] (similar dependences have been reported by [32]: $a = 170\ kJ\ mol^{-1}$ and $b = 0.146\ kJ\ K^{-1}\ mol^{-1}$, [33]: $a = 168\ kJ\ mol^{-1}$ and $b = 0.144\ kJ\ K^{-1}\ mol^{-1}$, and by [16]: $a = 164\ kJ\ mol^{-1}$ and $b = 0.139\ kJ\ K^{-1}\ mol^{-1}$). For the decomposition of $BaCO_3$: $a = 232\ kJ\ mol^{-1}$ and $b = 0.133\ kJ\ K^{-1}\ mol^{-1}$ [34] or $a = 243\ kJ\ mol^{-1}$ and $b = 0.143\ kJ\ K^{-1}\ mol^{-1}$ [35]. These values are relatively similar to those of the enthalpy and entropy changes at the reaction temperatures; for $CaCO_3$ decomposition at 550°C, $\Delta H^0 = 173\ kJ\ mol^{-1}$ and $\Delta S^0 = 0.154\ kJ\ K^{-1}\ mol^{-1}$ [31], and for $BaCO_3$ decomposition at 900°C, $\Delta H^0 = 235.1\ kJ\ mol^{-1}$ and $\Delta S^0 = 0.1355\ kJ\ K^{-1}\ mol^{-1}$ [34].

Despite the large number of works devoted to the study of the thermal decomposition of carbonates, to our knowledge, there are no works dedicated to analyze the decomposition of carbonates in the form of films. Knowing the mechanisms and kinetics governing the gas-solid state reactions involved in the synthesis of oxides is crucial to optimize film synthesis and control the final film morphology. Moreover, in powders the surface area of the reaction interface is not constant and there is often considerable uncertainty in its determination, whereas in films it is basically constant and well known. In addition, gas exchange is much faster in films than in powders, so the determination of the reaction mechanism is simpler. Besides, in powders it has been reported that the heat consumed by the decomposition and gas diffusion of the carbonate affects the kinetics [36–40]. In contrast, heat dissipation through the substrate is much more efficient in films so the effect on the kinetics of the heat absorbed or generated by the reaction is negligible [41, 42]. Moreover, the significantly faster heat transport in films compared to powders allows higher heating rates to be used, while avoiding the formation of temperature gradients within the sample.

In contrast, the sample masses involved in film analysis are usually quite small, in the order of a few hundredths of a milligram at best. Consequently, the signal obtained for kinetic analysis is very weak and sensitive to deviations of the baseline, experimental noise and experimental artifacts. Accordingly, it is difficult to obtain well-defined, low-noise transformation rate curves in which the peak shape is not affected by the choice of the baseline. Therefore, the use of advanced kinetic methods, such as isoconversional methods, is limited.

The decomposition kinetics of carbonate films has three distinct dependencies: the dependence of the reaction rate on temperature, its dependence on the carbon dioxide partial pressure and its dependence on film thickness. Furthermore, the carbon dioxide partial pressure dependence also involves the temperature through the equilibrium partial pressure, $g(p(CO_2))$. Since these dependencies are entangled, traditional kinetic approaches relying solely on temperature result in the scattered values for the reported activation energy.

In this work we introduce three complementary analyses enabling the separate determination of the functional dependence of the kinetics on the system parameters and to predict the onset of carbonate decomposition. The first analysis consists on determining the onset temperature as a function of $p(CO_2)$ to characterize $g(p(CO_2))$. The second analysis entails analyzing the decomposition of $CaCO_3$ and $BaCO_3$ films at very low $p(CO_2)$ (vacuum conditions) to determine the reaction rate. Finally, we explore the dependence of the kinetics on the film thickness. As a result, we were able to obtain a complete characterization of the functional dependence of the kinetics on the system parameters in a relatively simple and reliable way.

Materials and methods

The initial $CaCO_3$ and $BaCO_3$ films were characterized by Fourier transform infrared spectroscopy (FTIR) and X-ray diffraction (XRD). FTIR analysis was performed with a Bruker ALPHA spectrometer connected to an attenuated total reflectance module. XRD spectra were obtained with a Bruker AXS D8 ADVANCE diffractometer with a Cu-Kα source (1.5406 Å) operating at 40 kV and 40 mA.

Films were obtained by depositing through spin coating a solution of the metal propionate onto $10 \times 10\ mm^2$ $LaAlO_3$ (LAO) substrates and drying them at 70°C for 5 min. The starting solutions for $CaCO_3$ and for $BaCO_3$ were obtained by dissolving calcium propionate (Glentham ≥ 99%) and barium acetate (Sigma Aldrich ≥ 99%) in propionic acid (Merck, ≥ 99%), respectively. The solution was then kept under sonication until complete dissolution of the salt to a concentration $[M^{2+}] = 1.5M$. Removal of organic moieties was achieved after heating the films from

room temperature to 500°C at a heating rate of 5 K min^{-1} under a flow rate of 80 mL min^{-1} of wet oxygen [43, 44]. X-ray and FTIR analyses of the films (not shown) confirmed that the phases after pyrolysis of calcium propionate and barium propionate are calcite [44] and orthorhombic $BaCO_3$, respectively.

The nominal film thickness, h, given in this work is calculated from the mass of the films, the carbonate density (ρ_{CaCO_3}=2.71 g cm^{-3} and ρ_{BaCO_3}=4.29 g cm^{-3} [45]) and the surface area, S, of the substrate, $h = \frac{m}{\rho S}$. The nominal thickness is expected to be lower than the actual thickness due to porosity.

The decomposition of carbonate under vacuum conditions was carried out in a quartz tube surrounded by a low thermal inertia tube furnace, as shown in Fig. 1. An alumina sample holder is used to place the sample in the hot zone of the furnace. A thermocouple is placed in contact with the sample to measure its temperature. One end of the tube is connected to the carrier gas. The composition of the atmosphere is controlled by means of the carrier gas by mixing high purity N_2 and synthetic air (Air Liquide, $CO_2 \leq 1$ ppm and purity $\geq$ 99.999%) using MKS Instruments G-series mass flow controllers. The other end of the quartz tube is connected to a to a Leybold LEYSPEC view 100 S quadrupole mass analyzer in series with a turbomolecular pump and a rotary pump to drag the gas evolved from the sample and achieve the necessary vacuum (the total pressure at the sample chamber was around 10^{-4} mbar). The quadrupole mass analyzer allows to measure the CO_2 (m/z=44) partial pressure set by the carrier gas as well as recording the decomposition of carbonate as a function of temperature.

Carbonate decomposition at atmospheric pressure was performed on a Mettler Toledo thermobalance (TG), model TGA/DSC1. The determination of the $p(CO_2)$ inside the TG furnace was performed using the Leybold LEYSPEC quadrupole connected to the TG with a steel capillary and a needle valve.

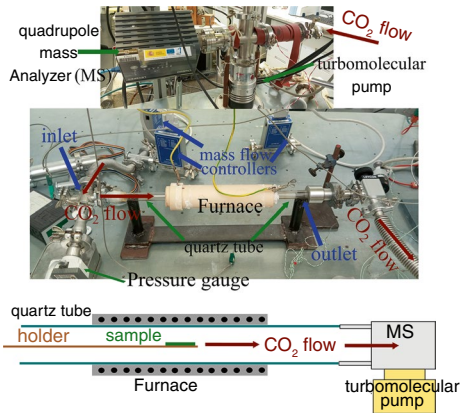

Fig. 1 Experimental set-up for measuring carbonate decomposition under vacuum conditions

Reaction models and kinetic analysis

Reaction models

As a first approximation, three basic models are candidates to describe the decomposition of carbonate: (i) the rate of decomposition is governed by the reaction at the interface or between the oxide and the carbonate, (ii) the rate of decomposition is governed by the diffusion of CO_2 through the oxide layer formed on top of the carbonate layer, and (iii) the oxide develops spontaneously at randomly distributed points throughout the film [3].

Interface limited decomposition

In reversible reactions, if diffusion is sufficiently fast, the reaction occurs on a reactant/product interface [46] and the kinetics is controlled by the forward and reverse reaction rate constants k_f and k_r, respectively. Thus, the number of moles of CO_2 evolved in a time interval dt is:

$$\frac{dn}{dt} = \frac{S}{R_G T}\left(k_f - k_r p(CO_2)\right). \tag{6}$$

where S is the film surface.

Since at equilibrium the reaction rate is zero:

$$k_r = \frac{k_f}{p_{eq}(CO_2)} \tag{7}$$

The evolution of the number of moles of CO_2 is:

$$\frac{dn}{dt} = k_f \frac{S}{R_G T}\left(1 - \frac{p(CO_2)}{p_{eq}(CO_2)}\right). \tag{8}$$

Moreover, since the surface area of the film S is constant, we can easily relate the number of evolved moles (dn = dm/M) to the degree of transformation (dα = dm/m):

$$d\alpha = dn\frac{M}{\rho h S}, \tag{9}$$

where M is the carbonate molecular mass, h is the initial film thickness and ρ is the carbonate density. Finally, assuming an Arrhenius dependence on temperature for k_f ($k_f = k_{f,0}e^{-\frac{E_f}{R_G T}}$) we obtain:

$$\frac{d\alpha}{dt} = k_{f,0}\frac{M}{\rho R_G T}\frac{1}{h}e^{-\frac{E_f}{R_G T}}\left(1 - \frac{p(CO_2)}{p_{eq}(CO_2)}\right). \tag{10}$$

where E_f and $k_{f,0}$ are the activation energy and the pre-exponential term of the forward rate constant.

Taking into account that the rate constant in Eq. 2 is $k(T) = Ae^{-\frac{E_f}{R_G T}}$, we obtain:

$$A = k_{f,0}\frac{M}{\rho R_G}\frac{1}{h}, \tag{11}$$

and

$$E_A = R_G T^2 \frac{\mathrm{d}\ln(k(T))}{\mathrm{d}T} = E_f - R_G T, \tag{12}$$

The activation energies for product recombination are generally low, so $E_f \approx \Delta H^0$ is expected [3] and the $R_G T$ term is about 5 kJ mol^{-1}, so $E_A \approx \Delta H^0$.

Diffusion limited decomposition

If diffusion through the layer is the limiting mechanism, then the reaction is fast enough to reach equilibrium at the interface, so the concentration of CO_2 at the interface, c_i, is that of equilibrium:

$$c_i = c_e = \frac{p_{eq}(CO_2)}{R_G T}. \tag{13}$$

If we assume that the concentration of CO_2 at the film surface is that of the surrounding atmosphere:

$$c_0 = \frac{p(CO_2)}{R_G T}. \tag{14}$$

And in stationary conditions the rate of evolution of CO_2 is:

$$\frac{1}{S}\frac{\mathrm{d}n}{\mathrm{d}t} = D\frac{c_e - c_0}{z} = \frac{D}{R_G T}\frac{p_{eq}(CO_2) - p(CO_2)}{z}. \tag{15}$$

where z is the thickness of the oxide along which CO_2 diffusion occurs and $D = D_0 e^{-E_d/R_G T}$ is the diffusion coefficient. And, if we take into account that $\alpha = z/h$ and that $\mathrm{d}n = \mathrm{d}m/M$ we obtain:

$$\frac{\mathrm{d}\alpha}{\mathrm{d}t} = D\frac{M}{\rho R_G T}\frac{1}{h^2}\frac{1}{\alpha}p_{eq}(CO_2)\left(1 - \frac{p(CO_2)}{p_{eq}(CO_2)}\right). \tag{16}$$

And taking into account that both diffusion and $p_{eq}(CO_2)$ are thermally activated, we obtain,

$$\frac{\mathrm{d}\alpha}{\mathrm{d}t} = D_0\frac{M}{\rho R_G T}\frac{1}{h^2}e^{-\frac{\Delta S^0}{R_G}}\frac{1}{\alpha}e^{-\frac{\Delta H^0 + E_d}{R_G T}}\left(1 - \frac{p(CO_2)}{p_{eq}(CO_2)}\right). \tag{17}$$

So the pre-exponential term and the activation energy are:

$$A = D_0\frac{M}{\rho R_G}\frac{1}{h^2}e^{-\frac{\Delta S^0}{R_G}}, \tag{18}$$

and

$$E_A = R_G T^2 \frac{\mathrm{d}\ln(k(T))}{\mathrm{d}T} = E_d + \Delta H^0 - R_G T, \tag{19}$$

Since the molar volume of the oxide is lower than that of the carbonate, the oxide film can be porous. In this case $E_d << \Delta H^0$ and $E_A \approx \Delta H^0$.

Random nucleation decomposition

Finally, if the decomposition is governed by random nucleation and growth of the new oxide phase throughout the film, the reaction rate does not depend on the film thickness and the activation energy depends on the nucleation and growth activation energies [47–50].

Note that, depending on the control mechanism, the pre-exponential term shows a different dependence on the film thickness; $A \propto h^{-n}$, where $n = 0$, 1 and 2 for a decomposition governed by nucleation and growth, by the interface reaction and by CO_2 diffusion, respectively. Furthermore, it is important to stress that for the advancing interface and CO_2 diffusion mechanisms the activation energy is similar to the enthalpy change of the reaction.

Kinetic analysis

The main drawback of working with layers is their low mass, so experimental artifacts and inaccuracies in TG and mass spectroscopy (MS) measurements significantly affect the shape of TG and MS curves. However, the onset temperature, T_{Onset} (T_{Onset} is the intersection point of the extrapolated baseline and the tangent at the beginning of the peak), and the temperature at which the transformation rate is maximum, T_{Kis}, can be determined with fair confidence. For this reason, the kinetic analyses are based on the determination of T_{Onset} or T_{Kis}.

Specifically, to determine the reaction rate we have performed Kissinger's analysis [51] which is based on the determination of the peak temperature, T_{Kis}, for experiments carried out at a constant heating rate, β. Kissinger's method assumes that the kinetics is governed by a single step reaction and is derived directly from Eq. 2 with $g(p(CO_2)) = 1$:

$$ln\left(\frac{\beta}{T_{Kis}^2}\right) = -\frac{E_A}{R_G T_{Kis}} + ln\left(-\frac{AR_G}{E_A}f'(\alpha_M)\right), \tag{20}$$

where α_M is the degree of transformation at T_{Kis}. The values of α_M and $f'(\alpha_M)$ for different reaction models are given in [52]. Thus, according to Eq. 20, the plot of $ln\left(\frac{\beta}{T_{Kis}^2}\right)$ versus the reciprocal of temperature should give a straight line from whose slope and intercept E_A and A can be determined.

Kissinger's method is exact for a first-order reaction and inaccuracies are less than 5% for many reaction models as long as $E_A/R_GT > 10$ [53] and for some models less than 1% for $E_A/R_GT > 30$ [54]. However, Kissinger's method has important limitations: it cannot be used to analyze processes occurring in cooling experiments [55], it is inaccurate for non-constant heating rate experiments [56], it fails for processes that do not obey the Arrhenius equation [57], and it does not give a reliable result when the process has multi-step kinetics that cannot be described by a single value of the activation energy [21].

As we will see below, $E_A/R_GT > 30$, so the only relevant consideration is to check that the process can be described approximately by a constant value of the activation energy. For this purpose we have used Friedman's exact isoconversional method [58]. Friedman's method is derived directly from the isoconversional principle which states that for a given degree of transformation α, the conversion rate is only a function of temperature. [59, 60]:

$$\left[\frac{\mathrm{dln}(\mathrm{d}\alpha/\mathrm{d}t)}{\mathrm{d}T^{-1}}\right]_\alpha = -\frac{E_\alpha}{R_G}, \tag{21}$$

where E_α is the activation energy at a given degree of transformation. The integration of Eq. 21 gives the transformation rate:

$$\frac{\mathrm{d}\alpha}{\mathrm{d}t} = A_\alpha f(\alpha)\exp\left[-\frac{E_\alpha}{R_GT}\right]. \tag{22}$$

To linearize Eq. 22 we apply logarithms to both sides:

$$\ln\frac{\mathrm{d}\alpha}{\mathrm{d}t} = -\frac{E_\alpha}{R_GT} + \left(A_\alpha f(\alpha)\right). \tag{23}$$

Therefore, for a given α, E_α can be determined from the slope of a plot of $\ln\frac{\mathrm{d}\alpha}{\mathrm{d}t}$ versus $1/T_\alpha$, where the set of data points $\frac{\mathrm{d}\alpha}{\mathrm{d}t}$ and T are obtained from experiments performed at different heating rates. To reduce the detrimental effect of noise in the Friedman analysis, we have applied a Savitzky-Golay filter [61], but taking care not to alter or distort the shape of the transformation rate curve.

Finally, to analyze the dependence of the pre-exponential term A on film thickness we use the following approximate solution of Eq. 20 [62]:

$$x_{\mathrm{Kis}} = x_0 + \frac{2x_0}{2+x_0}\ln\left(\frac{z}{z_0}\right), \tag{24}$$

where $x_{\mathrm{Kis}} = \frac{E_A}{R_GT_{\mathrm{Kis}}}$, $z = \frac{1}{2}\sqrt{-\frac{E_AA}{R_G\beta}f'(\alpha_M)}$ and x_0 is x_{Kis} for a given experiment, that is, for a particular heating rate β_0 and film thickness h_0.

Note that for different experiments performed on films of the same compound, all terms of the z parameter are identical except the heating rate and the pre-exponential term. According to Sect. 3.1 A depends on the thickness of the film, h; $A \propto h^{-n}$, where $n = 0, 1$ and 2 for a decomposition governed by nucleation and growth, advancing interface, and CO_2 diffusion, respectively. Therefore, if all experiments are performed at the same heating rate, the term $\frac{z}{z_0}$ reduces to $\left(\frac{h_0}{h}\right)^n$. In addition, as we will see in Sect. 4.1, for $BaCO_3$ and $CaCO_3$ decompositions $\frac{x_0}{2+x_0} \approx 0.94$, so Eq. 24 becomes:

$$\frac{1}{T_{\mathrm{Kis}}} = \frac{1}{T_0} + 0.94n\frac{R_G}{E_A}\ln\left(\frac{h_0}{h}\right), \tag{25}$$

where T_0 is the peak temperature for a thickness h_0. Thus, a plot of $\frac{1}{T_{\mathrm{Kis}}}$ versus $-0.94\frac{R_G}{E_A}\ln(h)$ should give a straight line of slope n. Therefore, this analysis will allow us to elucidate the decomposition mechanisms.

Results and discussion

Determination of the CO_2 equilibrium partial pressure

To determine the kinetic parameters of the Gibbs free energy, a and b in Eq. 5, we have performed TG measurements at a fixed heating rate for different CO_2 partial pressures. Since the kinetics depends on the film thickness, we have used films of similar thicknesses: for $CaCO_3$ the average film thickness was $0.43 \pm 0.03\mu$m while for $BaCO_3$ the average film thickness was $0.57 \pm 0.02\mu$m. The results for the decomposition of $CaCO_3$ and $BaCO_3$ are shown in Fig. 2. To determine the degree of transformation we assume that it is proportional to the mass, $m(t)$:

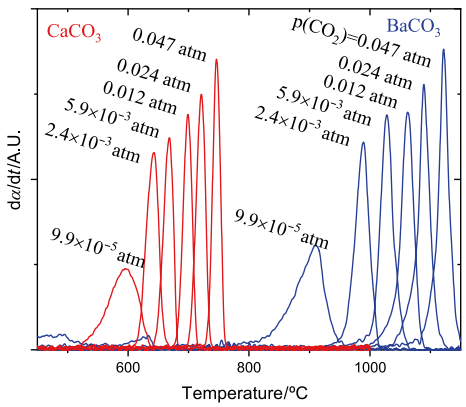

Fig. 2 Transformation rate determined from TG curves showing the decomposition evolution of $CaCO_3$ and $BaCO_3$ films when heated at a constant heating rate of 20 K min^{-1} for different CO_2 partial pressures

$$\alpha(t) = \frac{m(t) - m_f}{m_i - m_f}, \tag{26}$$

where m_i and m_f are the initial and final masses, respectively.

From Fig. 2, we can state that with increasing CO_2 partial pressure the peaks shift to higher temperatures and become narrower and sharper. This behavior is characteristic of reversible reactions [1, 16]. In fact, from Eqs. 2 and 3 it follows that the onset temperature, T_{Onset}, is the temperature at which the equilibrium pressure of CO_2 is equal to the external pressure. Thus, according to Eqs. 4 and 5, when $p(CO_2)$ increases, T_{Onset} also increases.

Moreover, a plot of $\ln(p(CO_2))$ with respect to the reciprocal of T_{Onset} should give a straight line. From the slope and intercept of this line we can determine the parameters a and b, respectively. This analysis has been performed in Fig. 3 and we have obtained for the $CaCO_3$ decomposition: $a = 174$ kJ mol^{-1} and $b = 0.148$ kJ K^{-1} mol^{-1} which are in very good agreement with [29, 31] ($a = 171$ kJ mol^{-1} and $b = 0.147$ kJ K^{-1} mol^{-1}). For the decomposition of $BaCO_3$ we obtain $a = 234$ kJ mol^{-1} and $b = 0.148$ kJ K^{-1} mol^{-1} which agree quite well with [34] ($a = 232$ kJ mol^{-1} and $b = 0.133$ kJ K^{-1} mol^{-1}). The small discrepancy in coefficient b for $BaCO_3$ may be related to the sorption of $p(CO_2)$ [17]. In Eq. 2 it is assumed that desorption and sorption are not rate-limiting steps for the forward and reverse reactions, respectively. These processes are related to the weak Van der Waals interaction between the solid and the CO_2 molecules, so the activation energy of sorption is much lower than that of $p_{eq}(CO_2)$, but the effect on entropy may be apparent [63].

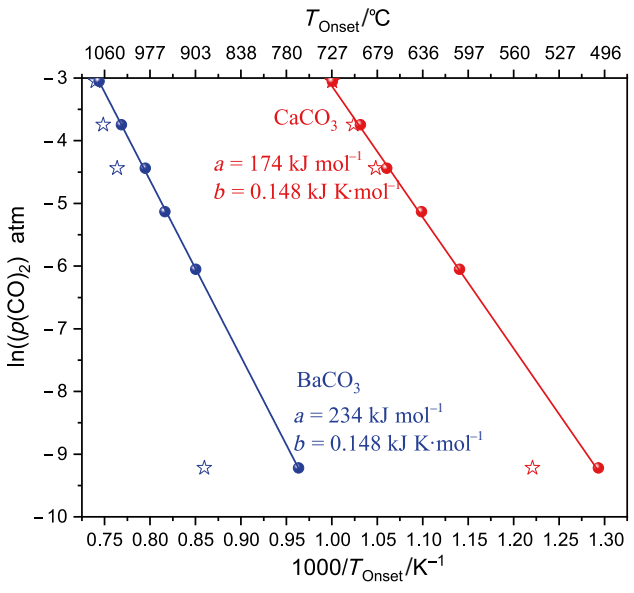

Fig. 3 Solid points: plot of $\ln(p(CO_2))$ with respect to $1000/T_{Onset}$ for the TG measurements shown in Fig. 2 from film decomposition. Empty stars: measurements made on samples in the form of powders

Therefore, if sorption controls the reverse reaction, then the onset temperature will be shifted to lower values and a slightly larger value of the b parameter will be obtained.

The agreement between the onset temperature in the films and the $p_{eq}(CO_2)$ by more than three orders of magnitude down to a $p(CO_2)$ as low as 9.9×10^{-5} atm shows that no CO_2-rich stagnant layer forms on the film surface. In contrast, the same analysis performed on powders (open stars in Fig. 3) shows that the formation of a local CO_2-rich atmosphere around the particles shifts the onset of decomposition to higher temperatures and, as expected, the effect of this local atmosphere is more relevant at low $p(CO_2)$. In fact, it has been shown that the gas transport is much faster in films [42, 64, 65] while the behavior of powders is affected by the formation of a local atmosphere around the particles [1]. Thus, in films the kinetics is not affected by the self-generated CO_2, whereas in the case of powders, total pressure, sample mass and powder compaction can have a significant effect on decomposition kinetics.

Kinetic analysis of the reaction rate constant

To determine the kinetic parameters and the influence of the $p(CO_2)$ on the activation energy, we have performed TG and MS experiments for two fixed $p(CO_2)$ and different heating rates. In Fig. 4 we have plotted the evolution of CO_2 when $BaCO_3$ films are heated at constant rates, β, of 5, 10, 15, 20, 30 and 40 K min^{-1} in vacuum ($p(CO_2) \approxeq 10^{-8}$ atm), the same measurements under the same vacuum conditions and for the same heating rates have been performed for $CaCO_3$ films. The thickness of the films remained approximately constant: the average film thickness was 0.56 ± 0.03μm and 1.03 ± 0.04μm for $CaCO_3$ and $BaCO_3$, respectively. We performed the same series of experiments at atmospheric pressure in the TG apparatus with a constant flow of 80 mL min^{-1} of high purity synthetic air. Due to furnace leakage, we have a

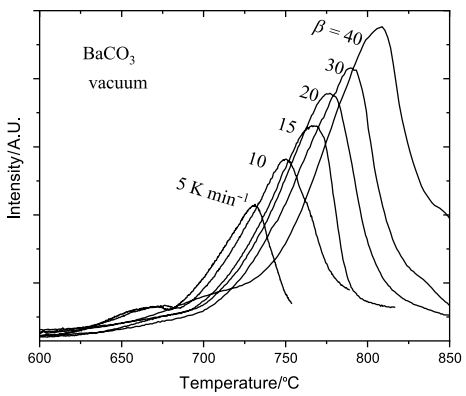

Fig. 4 MS curves showing the rate of CO_2 formation when $BaCO_3$ films are heated at different constant heating rates

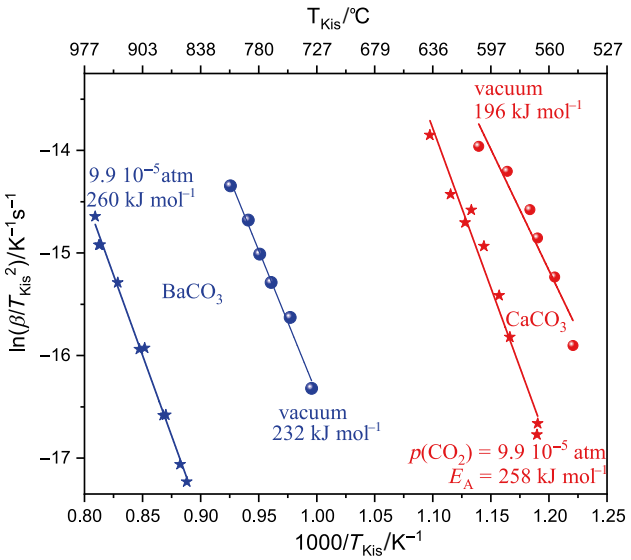

Fig. 5 Kissinger plots corresponding to the decomposition of $CaCO_3$ and $BaCO_3$ films in vacuum (circles) and at atmospheric pressure (stars). The continuous lines are the linear fit to Eq. 20

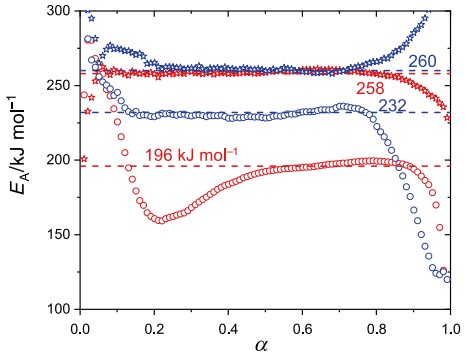

Fig. 6 Friedman analysis corresponding to the decomposition of $CaCO_3$ (blue symbols) and $BaCO_3$ (red symbols) films in vacuum (circles) and at atmospheric pressure (stars). The dashed lines are the activation energies obtained from the Kissinger analysis

significantly higher value of $p(CO_2)$, 9.9×10^{-5} atm. The Kissinger kinetic analysis of these four sets of experiments is shown in Fig. 5.

The experiments in vacuum have been performed at very low $p(CO_2)$ and according to Eq. 3 when $p(CO_2) \to 0$ then $g(p(CO_2)) \to 1$. Therefore, under vacuum conditions the reaction rate only depends on the parameters E_A and A. Thus, from the Kissigner analysis of the experiments done under vacuum conditions, Fig. 5, we can determine the activation energy of the rate constant. For $CaCO_3$ films we obtain an activation energy of 196 kJ mol^{-1}. This result is in good agreement with the results reported for $CaCO_3$ powders (191 kJ mol^{-1} in [16] and 195 kJ mol^{-1} in [66]) and single crystals (205 kJ mol^{-1} in [39]), both in vacuum. As for $BaCO_3$, we have obtained an activation energy of 232 kJ mol^{-1} that agrees well with the value of 226 kJ mol^{-1} for experiments performed in vacuum on single crystals [23]. Note that these activation energies are similar to the reaction enthalpies of $CaCO_3$ at 550°C (173 kJ mol^{-1}) and $BaCO_3$ at 900°C (235 kJ mol^{-1}), as expected according to Sect. 3.1 when the reaction is controlled by the reaction at the interface or by CO_2 diffusion.

To asses that the kinetics can be described approximately by a single value of the activation energy we have also performed Friedman's isoconvertional analysis, the result is shown in Fig. 6. The total mass evolved during carbonate decomposition is about 0.1 mg, as a result, the kinetic analysis is very sensitive to noise and experimental artifacts. In particular, the low baseline stability of the experiments dramatically affects the kinetic analysis for low and high degrees of conversion, this effect is especially noticeable for the decomposition of $BaCO_3$ in vacuum. Nevertheless, for the range of values where the Friedman analysis provides a reliable fit, we obtain a fairly constant value of the activation energy that matches the values obtained from the Kissinger analysis, so that, within the accuracy of our experiments, the kinetics can be described by a single value of the activation energy.

When $p(CO_2)$ is not negligible, the dependence of the kinetics on temperature is influenced by the function $g(p(CO_2))$ in Eq. 3. As a result, the activation energy determined from the kinetic analysis is not E_A, it is an apparent activation energy, E', which does not correspond to a physical parameter of the system. For this reason, the experiments performed at a $p(CO_2) = 9.9 \times 10^{-5}$ atm yield higher values of the activation energies, 258 and 260 kJ mol^{-1} for $CaCO_3$ and $BaCO_3$ respectively. In fact, the apparent activation energy, E', is known to increase with $p(CO_2)$ [29]:

$$E' = E_A + \Delta H^0 \times \frac{p(CO_2)}{p_{eq}(CO_2) - p(CO_2)}, \tag{27}$$

Note that when $p(CO_2) \to p_{eq}(CO_2)$, then $E' \to \infty$. For instance, for the decomposition of $CaCO_3$ Hashimoto [67] reported activation energies up to 1548 kJ mol^{-1} at a $p(CO_2) = 80$ kPa.

Therefore, even when working with high purity gases, the limited performance of commercial equipment for working in high purity environments may result in incorrect values of the activation energy [1, 16]. Furthermore, in the case of powder, the slower diffusion of CO_2 may also result in CO_2 accumulation. Therefore, kinetic analysis of powder can also result in higher values of the apparent activation energy. For $BaCO_3$ powders, an activation energy of 251 kJ mol^{-1} in nitrogen atmosphere [27] and 305 kJ mol^{-1} in argon atmosphere [25], respectively, has been reported.

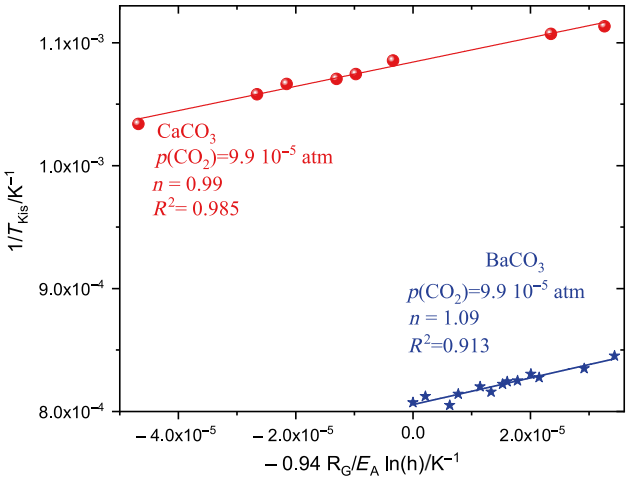

Fig. 7 Plot of $\frac{1}{T_{Kis}}$ versus $-0.94\frac{R_G}{E_A}\ln(h)$ for the decomposition of $CaCO_3$ and $BaCO_3$ films of different thicknesses heated at 30 K min^{-1}

Analysis of film thickness

As described in Sect. 3.2, we can determine the mechanism governing the decomposition by analyzing the dependence of the kinetics on film thickness. To this end, we have performed two sets of decomposition experiments, one for $CaCO_3$ and one for $BaCO_3$, which consist of determining the peak temperature for films of different thicknesses while keeping the heating rate constant. In addition, we need to determine the value of x_0 from a single experiment. For $CaCO_3$ we have T_0=650°C and E_A= 258 kJ mol^{-1} thus $x_0 = 33.6$ and for $BaCO_3$ we have T_0=810°C and E_A= 260 kJ mol^{-1} thus $x_0 = 28.9$, so for both the term $\frac{x_0}{2+x_0} \approx 0.94$. Then, according to Eq. 25 a plot of of $\frac{1}{T_{Kis}}$ with respect to $-0.94\frac{R_G}{E_A}\ln(h)$ should give a straight line whose slope is the n exponent of the pre-exponential factor.

In Fig. 7 we show the result of this plot and, in both cases, the data points are well aligned. We obtain values of n close to 1 (0.99 and 1.09 for $CaCO_3$ and $BaCO_3$, respectively) in agreement with a decomposition governed by the interface reaction. In fact, it has been reported that the interface reaction controls the decomposition of $CaCO_3$ in powders and in single crystals [2, 36, 37, 39, 68], where this interface consists of an active calcium oxide layer. The reason why diffusion is not the controlling mechanism is the formation of a porous oxide film due to the smaller molar volume of the oxide relative to that of the carbonate [2, 23, 39, 69].

For larger particles or coarser samples, diffusion of CO_2 through the oxide layer or transport of CO_2 out of the interparticle gaps may become the rate-limiting step. Moreover, according to Valverde [63], when $p(CO_2)$ is significant, the dependence of the active sites on temperature has to be taken into account and Eq. 2 is no longer valid. Besides, for large values of $p(CO_2)$ the temperature onset shifts to higher temperatures. In addition, increasing temperature and $p(CO_2)$ can alter the morphology and rate of decomposition. Thus, the activation energy determined at very low $p(CO_2)$ may not be valid for higher values of $p(CO_2)$. Still, it follows from Fig. 3 that the determination of the onset temperature is still valid over a relatively wide range of values of $p(CO_2)$.

Conclusions

To the best of our knowledge, in this work we have analyzed for the first time the decomposition kinetics of two carbonates in the form of films. We have analyzed the influence of $p(CO_2)$ on the onset temperature. We have shown that, in contrast to the powder, the kinetics is not affected by the self-generated CO_2 and the films exhibit a linear dependence of $\ln\left(p\left(CO_2\right)\right)$ on the reciprocal of the temperature.

In the case of $CaCO_3$ films there is a perfect agreement between this dependence and the dependence of the $p_{eq}\left(CO_2\right)$ with temperature, i.e., the decomposition reaction starts when the actual $p(CO_2)$ exceeds the equilibrium partial pressure. In the case of $BaCO_3$ films, the slope of this linear dependence agrees perfectly with the expected value determined from $p_{eq}\left(CO_2\right)$, but there is a slight difference in the value of the y-intercept. As a result, the onset is slightly shifted to lower temperatures relative to the expected value. This shift can be attributed to the sorption kinetics of CO_2.

In addition, we have characterized the rate constant from experiments performed under vacuum conditions. For both $CaCO_3$ and $BaCO_3$, the activation energies of the rate constant match the corresponding reaction enthalpy and agree with the reported activation energies from experiments performed at low $p(CO_2)$.

We have developed a new kinetic method that allows to analyze the dependence of the decomposition kinetics on film thickness. We have observed that the reaction rate is inversely proportional to the film thickness. This dependence reveals that the decomposition kinetics is controlled by the interface reaction and that the interface between the oxide and the carbonate advances from the top of the film to the substrate. CO_2 diffusion is not the rate-limiting mechanism, probably, due to the porosity of the oxide films and the relatively fast transport of the gas in the films.

Acknowledgments This work was funded by Spanish Ministry of Science, Innovation and Universities REBCOTLAG project (PID2021-127297OB-C22, co-financed by the European Regional Development Fund, MCIU/AEI/FEDER, UE) and by the Catalan Government, Generalitat of Catalunya, (2017-SGR-1519). Daniel Sanchez-Rodriguez acknowledges the support received from the Beatriu de Pinós Programme and the Ministry of Research and Universities of the Government of Catalonia (Fellowship BP00069). Open Access funding provided thanks to the CRUE-CSIC agreement with Springer. Authors thank the Scientific Services at UdG.

Author contributions Data collection and analysis were performed by ZS, GR, APl and DS-R. Experiment design and planning were performed by JF and DS-R. Kinetic Analysis and calculations were performed by JF and DS-R. JF wrote the manuscript. Scientific discussion and manuscript revision by DS-R, PR-G and MD.

Funding Open Access funding provided thanks to the CRUE-CSIC agreement with Springer Nature.

Declarations

Conflict of interest There are no conflict of interest to declare.

References

1. Hotta M, Tone T, Favergeon L, Koga N. Kinetic parameterization of the effects of atmospheric and self-generated carbon dioxide on the thermal decomposition of calcium carbonate. J Phys Chem C. 2022;126(18):7880–95.
2. Ingraham TR, Marier P. Kinetic studies on the thermal decomposition of calcium carbonate. Can J Chem Eng. 1963;41(4):170–3.
3. Brown M, Dollimore D, Galwey A. Theory of solid state reaction kinetics. In: Bamford CH, Tipper CFH, editors. Comprehensive chemical kinetics, reactions in the solid state, vol. 22. Amsterdam: Elsevier; 1980. p. 41–113.
4. Domone, P., Illston, J.: Construction materials: their nature and behaviour. In: Construction materials: their nature and behaviour, 4th ed., pp. 1–551. CRC Press, London (1973)
5. Oates JAH. Lime and limestone: chemistry and technology, production and uses. Berbyshire: CRC Press; 2008. p. 1–551.
6. Kavosh M, Patchigolla K, Anthony EJ, Oakey JE. Carbonation performance of lime for cyclic CO_2 capture following limestone calcination in steam CO_2 atmosphere. Appl Energy. 2014;131:499–507.
7. Arias B, Diego ME, Abanades JC, Lorenzo M, Diaz L, Martínez D, Alvarez J, Sánchez-Biezma A. Demonstration of steady state co_2 capture in a 1.7mwth calcium looping pilot. Int J Greenhouse Gas Control. 2013;18:237–45.
8. Ströhle J, Junk M, Kremer J, Galloy A, Epple B. Carbonate looping experiments in a 1 mw_{th} pilot plant and model validation. Fuel. 2014;127:13–22.
9. Arcenegui-Troya J, Sánchez-Jiménez PE, Perejón A, Moreno V, Valverde JM, Pérez-Maqueda LA. Kinetics and cyclability of limestone ($caco_3$) in presence of steam during calcination in the cal scheme for thermochemical energy storage. Chem Eng J. 2021;417: 129194.
10. Arcenegui Troya JJ, Moreno V, Sánchez-Jiménez PE, Perejón A, Valverde JM, Pérez-Maqueda LA. Effect of steam injection during carbonation on the multicyclic performance of limestone ($caco_3$) under different calcium looping conditions: a comparative study. ACS Sustain Chem Eng. 2022;10(2):850–9.
11. Arias B, Diego ME, Abanades JC, Lorenzo M, Diaz L, MartinezD, Alvarez J, Sanchez-Biezma A. Demonstration of steady state co2capture in a 1.7mwth calcium looping pilot. Int J Greenhouse Gas Control. 2013;18:237–245
12. Carmona-Quiroga PM, Blanco-Varela MT. Ettringite decomposition in the presence of barium carbonate. Cem Concr Res. 2013;52:140–8.
13. Soler L, Jareño J, Banchewski J, Rasi S, Chamorro N, Guzman R, Yáñez R, Mocuta C, Ricart S, Farjas J, Roura-Grabulosa P, Obradors X, Puig T. Ultrafast transient liquid assisted growth of high current density superconducting films. Nat Commun. 2020;11(1):344.
14. Buscaglia MT, Bassoli M, Buscaglia V, Alessio R. Solid-state synthesis of ultrafine $batio_3$ powders from nanocrystalline $baco_3$ and tio_2. J Am Ceram Soc. 2005;88(9):2374–9.
15. Bakken K, Pedersen VH, Blichfeld AB, Nylund I-E, Tominaka S, Ohara K, Grande T, Einarsrud M-A. Structures and role of the intermediate phases on the crystallization of BaTiO 3 from an aqueous synthesis route. ACS Omega. 2021;6(14):9567–76.
16. Criado JM, González M, Málek J, Ortega A. The effect of the CO_2 pressure on the thermal decomposition kinetics of calcium carbonate. Thermochim Acta. 1995;254:121–7.
17. Zawadzki J, Bretsznajder S. Some remarks on the mechanism of reactions of the type: solid=solid + gas. Trans Faraday Soc. 1938;34:951–9.
18. Khinast J, Krammer GF, Brunner C, Staudinger G. Decomposition of limestone: the influence of CO_2 and particle size on the reaction rate. Chem Eng Sci. 1996;51(4):623–34.
19. Criado JM, Ortega A. A study of the influence of particle size on the thermal decomposition of $CaCO_3$ by means of constant rate thermal analysis. Thermochim Acta. 1992;195:163–7.
20. Cui Z, Xue Y, Xiao L, Wang T. Effect of particle size on activation energy for thermal decomposition of nano-$CaCO_3$. J Comput Theor Nanosci. 2013;10(3):569–72.
21. Vyazovkin S, Burnham AK, Criado JM, Pérez-maqueda LA, Popescu C, Sbirrazzuoli N. ICTAC Kinetics Committee recommendations for performing kinetic computations on thermal analysis data. Thermochim Acta. 2011;520(1–2):1–19.
22. Maciejewski M, Reller A. How (UN)reliable are kinetic data of reversible solid-state decomposition processes? Thermochim Acta. 1987;110:145–52.
23. Basu TK, Searcy AW. Kinetics and thermodynamics of decomposition of barium carbonate. J Chem Soc Faraday Trans 1 Phys Chem Condens Phases. 1976;72:1889.
24. Acharya SG, Bhatia SK, Shankar HS. Kinetics of solid state reaction between barium carbonate and cupric oxide. Metall Trans B. 1992;23(4):493–503.
25. Arvanitidis I, Siche D, Seetharaman S. A study of the thermal decomposition of BaCO3. Metall Mater Trans B. 1996;27(3):409–16.
26. Maitra S, Bandyopadhyay N, Das S, Pal AJ, Pramanik J. Non-isothermal decomposition kinetics of alkaline earth metal carbonates. J Am Ceram Soc. 2007;90(4):1299–303.
27. Hancock, J.D.: Solid state reactions of barium carbonate with tetravalent metal oxides. PhD thesis, University of Sheffield (1970)
28. Judd MD, Pope MI. Energy of activation for the decomposition of the alkaline-earth carbonates from thermogravimetric data. J Therm Anal. 1972;4(1):31–8.
29. Vyazovkin S. Kinetic effects of pressure on decomposition of solids. Int Rev Phys Chem. 2020;39(1):35–66.
30. Koga N, Vyazovkin S, Burnham AK, Favergeon L, Muravyev NV, Pérez-Maqueda LA, Saggese C, Sánchez-Jiménez PE. ICTAC kinetics committee recommendations for analysis of

thermal decomposition kinetics. Thermochim Acta. 2023;719: 179384.
31. Barin I, Knacke O, Kubaschewski O. Thermochemical properties of inorganic substances. Berlin: Springer; 1973. p. 922.
32. Silcox GD, Kramlich JC, Pershing DW. A mathematical model for the flash calcination of dispersed calcium carbonate and calcium hydroxide particles. Ind Eng Chem Res. 1989;28(2):155–60.
33. Hill KJ, Winter ERS. Thermal dissociation pressure of calcium carbonate. J Phys Chem. 1956;60(10):1361–2.
34. Chang YA, Ahmad N. Thermodynamic data on metal carbonates and related oxides. Warrendale: Metallurgical Society of AIME; 1982. p. 235.
35. Lindemer TB, Specht ED. The BaO-Cu-CuO system. Solid-liquid equilibria and thermodynamics of BaCuO2 and BaCu2O2. Phys C Supercond. 1995;255(1–2):81–94.
36. Hills AWD. The mechanism of the thermal decomposition of calcium carbonate. Chem Eng Sci. 1968;23(4):297–320.
37. Britton HTS, Gregg SJ, Winsor GW. The calcination of dolomite. Part I.-The kinetics of the thermal decomposition of calcite and of magnesite. Trans Faraday Soc. 1952;48:63–9.
38. Rouquerol J. Critical examination of several problems typically found in the kinetic study of thermal decomposition under vacuum. J Therm Anal. 1973;5(2–3):203–16.
39. Beruto D, Searcy AW. Use of the Langmuir method for kinetic studies of decomposition reactions: calcite ($CaCO_3$). J Chem Soc Faraday Trans 1 Phys Chem Condens Phases. 1974;70:2145.
40. Caldwell KM, Gallagher PK, Johnson DW. Effect of thermal transport mechanisms on thermal-decomposition of $CaCO_3$. Thermochim Acta. 1977;18(1):15–9.
41. Sánchez-Rodríguez D, Eloussifi H, Farjas J, Roura P, Dammak M. Thermal gradients in thermal analysis experiments: criterions to prevent inaccuracies when determining sample temperature and kinetic parameters. Thermochim Acta. 2014;589:37–46.
42. Roura P, Farjas J, Eloussifi H, Carreras L, Ricart S, Puig T, Obradors X. Thermal analysis of metal organic precursors for functional oxide preparation: thin films versus powders. Thermochim Acta. 2015;601:1–8.
43. Rasi S, Ricart S, Obradors X, Puig T, Roura-Grabulosa P, Farjas J. Radical and oxidative pathways in the pyrolysis of a barium propionate-acetate salt. J Anal Appl Pyrolysis. 2019;141: 104640.
44. Zaidi S, Sánchez-Rodríguez D, Farjas J, Dammak M, Roura-Grabulosa P. Thermal decomposition of calcium propionate: films and powders. J Therm Anal Calorim. 2023;148:13039–49.
45. Lide DR, Frederikse HPR. CRC handbook of chemistry and physics: a ready-reference of chemical and physical data. Boca Raton: CRC Press; 2002.
46. Galwey AK, Brown ME. Application of the Arrhenius equation to solid state kinetics: Can this be justified? Thermochim Acta. 2002;386(1):91–8.
47. Avrami M. Kinetics of phase change. I general theory. J Chem Phys. 1939;7(12):1103–12.
48. Avrami M. Kinetics of phase change. II Transformation-time relations for random distribution of Nuclei. J Chem Phys. 1940;8(2):212.
49. Avrami M. Granulation, phase change, and microstructure: kinetics of phase change. III J Chem Phys. 1941;9(2):177–84.
50. Erofe'ev BV. Generalized equation of chemical kinetics and its application in reactions involving solids. CR Dokl Acad Sci URSS. 1946;52:511.
51. Kissinger HE. Reaction kinetics in differential thermal analysis. Anal Chem. 1957;29(11):1702–6.
52. Farjas J, Roura P. Simple approximate analytical solution for nonisothermal single-step transformations: kinetic analysis. AIChE J. 2008;54(8):2145–54.
53. Budrugeac, P., Segal, E.: Applicability of the Kissinger equation in thermal analysis revisited. J Therm Anal Calorimetry; 9th Eur Symp Therm Anal Calorim 88(3): 703–707 (2007)
54. Criado JM, Ortega A. Non-isothermal transformation kinetics: remarks on the Kissinger method. J Non Cryst Solids. 1986;87(3):302–11.
55. Vyazovkin S. Is the Kissinger equation applicable to the processes that occur on cooling? Macromol Rapid Commun. 2002;23(13):771–5.
56. Vyazovkin S. Kissinger method in kinetics of materials: things to beware and be aware of. Molecules. 2020;25(12):2813.
57. Baumann W, Leineweber A, Mittemeijer EJ. Failure of Kissinger(-like) methods for determination of the activation energy of phase transformations in the vicinity of the equilibrium phase-transformation temperature. J Mater Sci. 2010;45(22):6075–82.
58. Friedman HL. Kinetics of thermal degradation of char-forming plastics from thermogravimetry. Application to a phenolic plastic. J Polym Sci Part C Polym Symp. 1964;6(1):183–95.
59. Vyazovkin S, Wight CA. Isothermal and nonisothermal reaction kinetics in solids: in search of ways toward consensus. J Phys Chem A. 1997;101(44):8279–84.
60. Farjas J, Roura P. Isoconversional analysis of solid state transformations. A critical review Part II. Complex transformations. J Therm Anal Calorim. 2011;105(3):767–73.
61. Press WH, Flannery BP, Teukolsky SA, Vetterling WT. Numerical recipes in C: the art of scientific computing, vol. 2nd. Cambridge: Cambridge University Press; 1994. p. 994.
62. Farjas J, Roura P. Exact analytical solution for the Kissinger equation: determination of the peak temperature and general properties of thermally activated transformations. Thermochim Acta. 2014;598:51–8.
63. Valverde JM. On the negative activation energy for limestone calcination at high temperatures nearby equilibrium. Chem Eng Sci. 2015;132:169–77.
64. Roura P, Farjas J, Ricart S, Aklalouch M, Guzman R, Arbiol J, Puig T, Calleja A, Peña-Rodríguez O, Garriga M, Obradors X. Synthesis of nanocrystalline ceria thin films by low-temperature thermal decomposition of Ce-propionate. Thin Solid Films. 2012;520(6):1949–53.
65. Sanchez-Rodriguez D, Farjas J, Roura P, Ricart S, Mestres N, Obradors X, Puig T. Thermal analysis for low temperature synthesis of oxide thin films from chemical solutions. J Phys Chem C. 2013;117(39):20133–8.
66. Farjas J, Butchosa N, Roura P. A simple kinetic method for the determination of the reaction model from non-isothermal experiments. J Therm Anal Calorim. 2010;102(2):615–25.
67. Hashimoto H. The thermal decomposition of calcium carbonate(II) the effect of carbon dioxide. J Soc Chem Ind Jpn. 1961;64(7):1162–6.
68. Valverde JM, Sanchez-Jimenez PE, Perez-Maqueda LA. Limestone calcination nearby equilibrium: kinetics, CaO crystal structure, sintering and reactivity. J Phys Chem C. 2015;119(4):1623–41.
69. Beruto D, Barco L, Searcy AW, Spinolo G. Characterization of the porous CaO particles formed by decomposition of CaCO3 and Ca(OH)2 in vacuum. J Am Ceram Soc. 1980;63(7–8):439–43.